

RESEARCH ARTICLE

On the Correlation Between Incident Power Density and Temperature Increase for Exposures at Frequencies Above 6 GHz

VALERIO DE SANTIS¹, (Senior Member, IEEE), ANTONIO DI FRANCESCO²,
GIORGI BIT-BABIK³, (Senior Member, IEEE), JOHN ROMAN⁴, (Senior Member, IEEE),
AND WALID EL HAJJ⁵, (Member, IEEE)

¹Department of Industrial and Information Engineering and Economics, University of L'Aquila, 67100 L'Aquila, Italy

²Department of Information Engineering, Computer Science and Mathematics, University of L'Aquila, 67100 L'Aquila, Italy

³Motorola Solutions Inc., Fort Lauderdale, FL 33322, USA

⁴Intel Corporation, Hillsboro, OR 97124, USA

⁵Wireless RF Laboratory, Intel Corporation, 06600 Antibes, France

Corresponding author: Valerio De Santis (valerio.desantis@univaq.it)


This work was supported in part by the Mobile & Wireless Forum.

ABSTRACT International guidelines/standards for human exposure to electromagnetic fields have recently been revised to update the dosimetric reference limits (DRLs or basic restrictions) and exposure reference levels (ERLs), specifically for frequencies above 6 GHz. At such frequencies, the ERL is defined in terms of incident power density (IPD) and used as a practical quantity to assess compliance with DRLs (absorbed or epithelial power density) and therefore appropriately limits temperature elevation at the body surface. In the exposure standards, IPD is spatially averaged over an area of 4 cm² below 30 GHz and 1 cm² above 30 GHz, however the definition of IPD is given in a theoretical manner. With the progress in the development of product safety compliance assessment standards, one concern has been how to define the IPD considering practical measurement procedures. Two definitions or averaging methods were considered: using IPD vectors normal to the averaging surface and using magnitude (norm) of IPD vectors. As the exposure guidelines are intended to prevent excessive tissue heating, statistical analysis was therefore undertaken to investigate which IPD metric better correlates with the temperature increase. To this end, a large data set for several exposure scenarios was collected by different research institutions. The analysis of the obtained results is presented and shows that both definitions have high correlation with temperature rise, with slightly better correlation (0.9 vs. 0.8) for the definition using the magnitude of IPD vectors.

INDEX TERMS 5G exposure, heating factor, human safety standard, power density, statistical analysis.

I. INTRODUCTION

With the advent of fifth-generation (5G) mobile devices, assessment of electromagnetic (EM) field exposure at frequencies above 6 GHz is receiving much consideration [1]. At these frequencies, often referred as millimeter-waves (mm-Waves), the established adverse effect on biological tissues is of thermal nature, related to a temperature increase of the superficial tissues, mainly skin and eye [2]–[5].

The associate editor coordinating the review of this manuscript and approving it for publication was Dost Muhammad Khan .

International exposure guidelines/standards for human protection from high-frequency electromagnetic fields have been recently revised by the International Commission on Non-Ionizing Radiation Protection (ICNIRP) [6] and the Institute of Electrical and Electronics Engineers (IEEE), with the International Commission on Electromagnetic Safety (ICES) under the Technical Committee (TC) 95 [7].

The use of the absorbed/epithelial power density (A/E-PD) as the basic restriction (BR) [6] or dosimetric reference limit (DRL) [7] for the frequencies above 6 GHz is one of the main changes in the guidelines/standards. Furthermore, the incident power density (IPD) in free space is

defined as the reference level (RL) [6] or exposure reference level (ERL) [7]. It should be noted that at mm-Waves, IPD is a more practical and straightforward measurand than the A/E-PD.

Based on the exposure guidelines/standards, the IPD should be averaged over a squared area of 4 cm^2 for frequencies from 6 to 300 GHz. However, for frequencies higher than 30 GHz, additional criteria of IPD averaged over 1 cm^2 are given with a relaxation of RL/ERL by a factor of 2 for local beam-like exposures [6], [7]. Since no technical specifications have been provided on how to determine these spatial averaging, some product compliance assessment standards have been established by the International Electrotechnical Commission (IEC) TC106 and IEEE ICES TC34 committees. These dual-logo standards, recently published, provide experimental and numerical procedures to assess exposure to IPD from 6 GHz to 300 GHz [8], [9].

Beside the averaging technique, one of the goals in the development of these assessment standards has been the definition of a robust IPD metric considering practical aspects of laboratory measurement procedures. Two definitions have been proposed so far:

- the first definition, where only *normal* components of the Poynting vector crossing the surface are used (sPD_n);
- the second definition, where all *total* components (i.e., magnitude) of the Poynting vector are considered (sPD_{tot}).

More recently, a third definition of IPD (i.e., including the reactive components of the Poynting vector) was proposed in [10], without however considering its relationship with tissue temperature rise. Since the exposure safety guidelines/standards are established to limit tissue heating, the main criterion for evaluating suitability of a particular IPD metric for compliance should be based on the correlation of that metric with temperature rise and therefore the latter definition has not been hereby considered. To summarize, the above two definitions were used to derive different IPD quantities for compliance by spatial averaging over 1 cm^2 as well as 4 cm^2 of the exposure evaluation surface, thus producing four different metrics.

The effect of the IPD definition as well as the IPD averaging method on the relationship between the resulting compliance quantity and the temperature rise have been studied in several publications [11]–[23]. However, the influence of these IPD definitions on the temperature correlation was not considered. Moreover, in the near-field and for oblique incidence, these definitions lead to different values with significant differences in some exposure conditions [24]–[26]. Therefore, it becomes necessary to study both definitions in terms of correlation with surface temperature elevation.

A new working group (WG) 5 under Subcommittee (SC) 6 of IEEE ICES TC95 has been established to clarify these aspects. A large amount of data from different independent

institutions were collected to study the IPD metric correlation with the surface temperature elevation in the frequency range from 6 to 300 GHz, which is essential for compliance assessment of new 5G wireless products.

This paper shows the results of the statistical analysis performed by the WG on the collected data, as well as some discussions and conclusions.

II. DATA COLLECTION

Six different organizations collaborated to perform the inter-comparison study [27]: the National Institute of Information and Communications Technology (NICT), Nagoya Institute of Technology (NITech), South China Agricultural University (SCAU), Dassault Systèmes SIMULIA (3DS), Foundation for Research on Information Technologies in Society (IT'IS), and the University of Split (UniSplit). The evaluation of the results started with the data collection and its structured aggregation. The data consisted of a total of 227 samples, obtained by combining the results from each participating institution who performed computer simulations of different exposure scenarios. Those simulations included the stratified tissue block models with various EM sources like dipole antennas, patch antennas and different antenna arrays at frequencies $f = 10, 30, 60$ and 90 GHz as well as a number of separation distances d between the source and body model set to 2, 5, 10, 50 and 150 mm. Each sample, corresponding to one particular simulation scenario, contained the computed peak values of spatially averaged PD (i.e., $psPD_n$ and $psPD_{tot}$ averaged over 1 cm^2 and 4 cm^2), the peak temperature increase $p\Delta T$, as well as the corresponding heating factors (HFs). The latter is defined as in [28]:

$$HF_{j,avg,k} = \frac{ps\Delta T}{psPD_{j,avg,k}}, \quad j = \{n, tot\}, k = \{1, 4\} \quad (1)$$

All participants of the study have provided the results for the dipole antennas, while results for EM sources made of directional antennas were provided by some of the groups. Therefore, the statistical analysis has been performed on two macro-groups or data sets made of:

- 115 samples for the dipole sources at all simulated distances and frequencies, referred to as *dipole data*;
- 112 samples for directional antennas sources at all simulated distances and frequencies, referred to as *directional antennas data*.

Among the latter, 46 samples come from dipole or patch array antennas with a beam shift in azimuth or elevation.

III. STATISTICAL CORRELATION ANALYSIS

A. SCATTER PLOTS

The first analysis has been conducted to visualize the scatter plots of the peak spatial-averaged power densities, $psPD$, and the respective relative values of peak temperature increase, $p\Delta T$. Specifically, the following pairs of data series have

been analyzed, first for *dipole data*, then for *directional antennas data*:

- ($psPD_n$ avg.1, $p\Delta T$);
- ($psPD_{tot}$ avg.1, $p\Delta T$);
- ($psPD_n$ avg.4, $p\Delta T$);
- ($psPD_{tot}$ avg.4, $p\Delta T$).

To evaluate possible influence of near-field exposure conditions, a distinction has been made by excluding the data coming from the simulations with distance $d = 2$ mm (i.e., $d \geq 5$ mm) and the data from all other simulation scenarios, i.e. $d \geq 2$ mm. The scatter plots were aimed at visually establishing the type of correlation (linear or not) and its strength (i.e., strong, weak or no correlation).

B. STANDARD DEVIATIONS OF HF

After generating the scatter plots for all data series, the HFs have been analyzed grouping the results by institution/group. To this end, the average value (μ_{HF}) and standard deviation (σ_{HF}) for every group have been computed for each of the four metrics, namely HF_n avg.1, HF_{tot} avg.1, HF_n avg.4 and HF_{tot} avg.4. The same computations were also performed considering the data from all groups together. The standard deviation of each HF sample was of particular interest, since a smaller value of σ_{HF} would suggest stronger correlation with ΔT . Finally, for each PD metric, the histograms of the HF data (computed for all the data sets) have been plotted to examine their distribution around the average value μ_{HF} .

C. PEARSON CORRELATION COEFFICIENTS

The analysis of the Pearson correlation coefficients has been performed to identify the PD metric that best correlates with the temperature increase ΔT . Specifically, the following Pearson correlation coefficients were evaluated:

- r_{n1} = Pearson coefficient of the pair ($psPD_n$ avg.1, $p\Delta T$);
- r_{tot1} = Pearson coefficient of the pair ($psPD_{tot}$ avg.1, $p\Delta T$);
- r_{n4} = Pearson coefficient of the pair ($psPD_n$ avg.4, $p\Delta T$);
- r_{tot4} = Pearson coefficient of the pair ($psPD_{tot}$ avg.4, $p\Delta T$).

Equation (2) was employed for the computation of the correlation coefficients [29]:

$$r_{jk} = \frac{Cov(psPD_j \text{ avg.}k, p\Delta T)}{\sigma(psPD_j \text{ avg.}k) \sigma(p\Delta T)}, \quad j = \{n, \text{tot}\}, k = \{1, 4\} \quad (2)$$

where $Cov(psPD_j \text{ avg.}k, p\Delta T)$ is the covariance of $psPD_j$ avg.k and $p\Delta T$, while $\sigma(psPD_j \text{ avg.}k)$ and $\sigma(p\Delta T)$ are the standard deviations of $psPD_j$ avg.k and $p\Delta T$, respectively. Each set of four different r_{jk} was computed considering the distinction between data obtained without including the separation distance $d = 2$ mm and all other data, namely:

- $r_{n1}, r_{tot1}, r_{n4}, r_{tot4}$ for *dipole* and $d \geq 5$ mm;
- $r_{n1}, r_{tot1}, r_{n4}, r_{tot4}$ for all *dipole data*;

- $r_{n1}, r_{tot1}, r_{n4}, r_{tot4}$ for *directional antennas* and $d \geq 5$ mm;
- $r_{n1}, r_{tot1}, r_{n4}, r_{tot4}$ for all *directional antennas data*.

Each of the four analyses above has been performed on data groups distinguished by the working frequency of the sources. Specifically, correlation coefficients have been computed first for all the available frequencies ($f = 10, 30, 60, 90$ GHz), then for the $f = 10, 30$ GHz set and finally for the $f = 60, 90$ GHz set, still distinguishing between dipole and directional antennas data. A clear picture of the analysed data groups is given in Tables 3 and 4 in Sec.IV.C.

D. STATISTICAL SIGNIFICANCE TEST

Finally, a statistical significance test was carried out to quantify the difference between the correlation coefficients and analyze values of r_{jk} , $j = \{n, \text{tot}\}$, $k = \{1, 4\}$ in a consistent and objective manner [30]. Such a procedure is also helpful to check whether the noise in the analyzed data had significant effect on the computed values of r_{jk} . In particular, it could be determined if the probability that the difference between r_{ap} and r_{bq} , $a \neq b$, is merely due to chance (i.e., noise in the data) with a predefined significance level α (e.g., $\alpha = 5\%$ if a confidence level of 95% is chosen). A simplified scheme of the statistical hypotheses for the testing procedure hereby adopted is described as follows:

1. Define the *null* and *alternative hypotheses*. In this analysis, the null hypothesis is defined as $H_0: \rho_{ap} = \rho_{bq}$, $a \neq b$ or $p \neq q$, where ρ_{ap} and ρ_{bq} are the **true** correlation coefficients of the pairs of data samples (sPD_a avg.p, ΔT) and (sPD_b avg.q, ΔT), while r_{ap} and r_{bq} are their estimators. The alternative hypothesis is defined as $H_1: \rho_{ap} > \rho_{bq}$, a, b, p, q such that $\rho_{ap} > \rho_{bq}$.
2. Employ an appropriate significance test, together with a relevant test statistic. Since the compared correlations have one variable in common (i.e., ΔT), the adopted test statistics for dependent correlations are those provided by the *cocor* package [30].
3. Choose the significance level α . In this analysis, a value of $\alpha = 5\%$ has been adopted.
4. Compute the values of z -scores or t -scores (i.e., the test statistics) associated to the difference $r_{ap} - r_{bq}$ based on the observed data.
5. Reject the null hypothesis H_0 in favour of the alternative hypothesis H_1 if the observed value $r_{ap} - r_{bq}$ is in the critical region; “fail to reject” (retain) H_0 otherwise.

The last two steps of the testing process are automatically performed by the tool provided in the *cocor* package [30]. Results in terms of z -scores or t -scores for each of the nine different applied tests are reported in Sec. IV.D.

The procedure above was applied to compare the performance of the normal and total component definitions in terms of correlation with ΔT , distinguishing the compared coefficients by the averaging area.

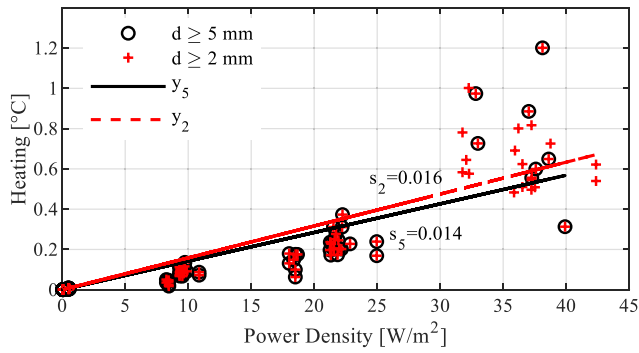


FIGURE 1. psPD_n avg.1 vs. pΔT dipole data scatter plot.

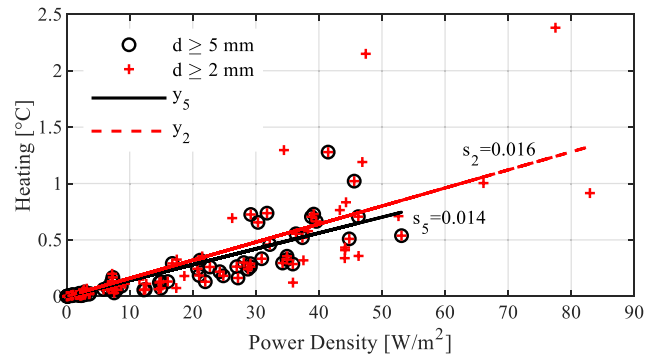


FIGURE 5. psPD_n avg.1 vs. pΔT directional antennas data scatter plot.

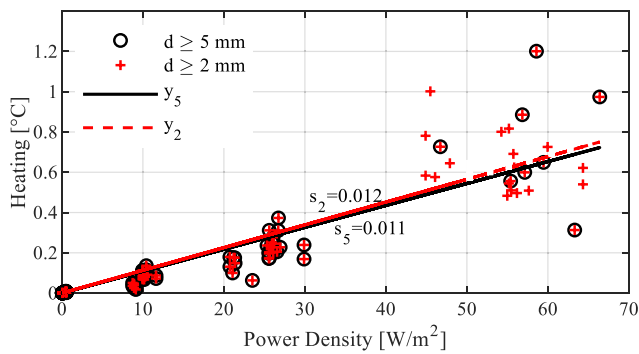


FIGURE 2. psPD_{tot} avg.1 vs. pΔT dipole data scatter plot.

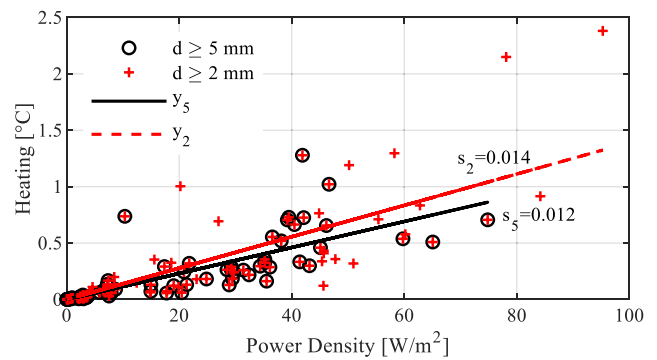


FIGURE 6. psPD_{tot} avg.1 vs. pΔT directional antennas data scatter plot.

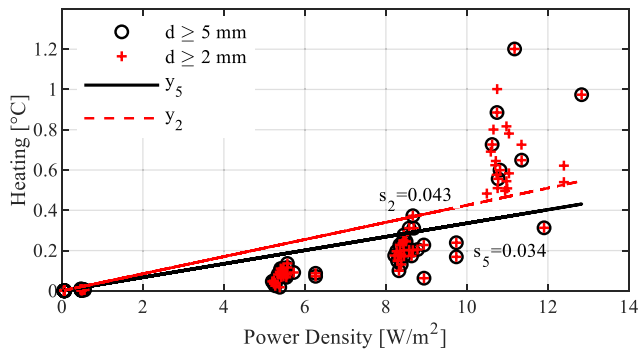


FIGURE 3. psPD_n avg.4 vs. pΔT dipole data scatter plot.

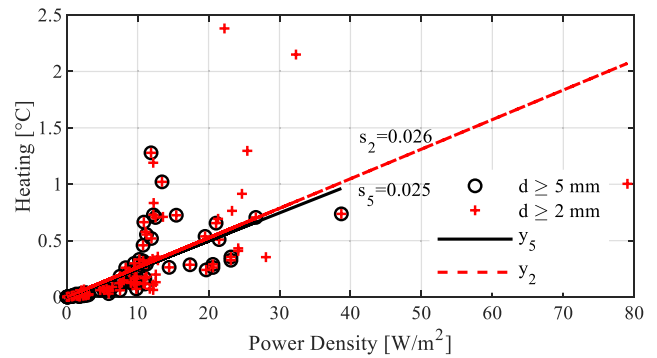


FIGURE 7. psPD_n avg.4 vs. pΔT directional antennas data scatter plot.

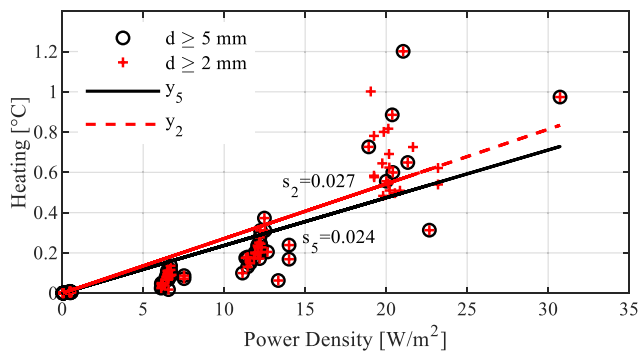


FIGURE 4. psPD_{tot} avg.4 vs. pΔT dipole data scatter plot.

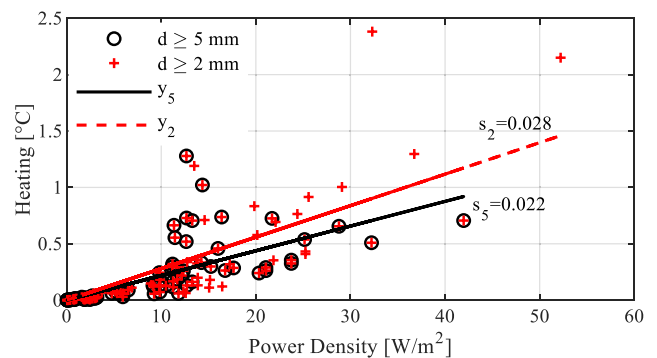


FIGURE 8. psPD_{tot} avg.4 vs. pΔT directional antennas data scatter plot.

IV. STATISTICAL RESULTS

A. SCATTER PLOTS

The scatter plots for the dipole and directional antennas are reported in Figs. 1-4 and 5-8, respectively.

It should be noted as regression lines given by the equation $y_i = s_i x$, with $i = \{5, 2\}$ referring to data with $d \geq 5$ mm or

TABLE 1. HF relative standard deviations [%] sorted by PD metrics. Highlighted in bold are the smallest values for each research group.

	σ (HF _n avg. 1)	σ (HF _{tot} avg. 1)	σ (HF _n avg. 4)	σ (HF _{tot} avg. 4)
NICT	61.67	51.82	71.00	60.68
NITech	46.72	49.26	90.05	92.88
SCAU	44.06	43.94	84.97	83.67
3DS	44.53	40.08	81.96	53.75
IT'IS	35.19	34.34	73.88	46.35
UniSplit	62.44	47.68	96.14	69.84
All data	57.02	49.58	90.09	76.95

TABLE 2. Ratio of 95th to 5th percentile for the four HF definitions. Highlighted in bold are the smallest values for each metric.

	HF _n avg. 1	HF _{tot} avg. 1	HF _n avg. 4	HF _{tot} avg. 4
Ratio	5.72	5.18	11.22	7.77

$d \geq 2$ mm, have been included in these plots. They provide insight into the collected data spread amongst the several institutions and simulation case studies, noting sporadic high values of HFs for some of the directional antennas, with particular reference to a pair of values with $p\Delta T$ between 2 and 2.5 °C (see Figs. 5-8). These values correspond to patch array antennas with a beam shift in azimuth or elevation, which have already been reported to exhibit a large spread of HFs [24]–[26]. A quantification of possible effects of these data on the Pearson correlation coefficients is given in Sec. IV.C (see Tables 3-6).

B. RELATIVE STANDARD DEVIATIONS OF HF

The relative standard deviations of the HF obtained for the several PD definitions and metrics from the several research groups are summarized in Table 1. It can be observed from this Table that the $psPD_{tot}$ definition always gives the HF distributions with the least relative standard deviations, except for the case of data provided by NITech group, where for the $psPD_n$ definition it is slightly smaller.

The histograms of the HF distributions are shown in Figs. 9-12. The average value of each distribution is demarked with a red dotted vertical line. The occurrence distributions show a noticeable positive skewness in all four cases. Thus, the ratio of the 95th to the 5th percentiles of the HF distributions has been performed to quantify the skewness and the tail length [27]. The computed ratios for each of the four HF definitions are reported in Table 2. Considering that the $psPD_{tot}$ values are in general higher than the $psPD_n$ while the $p\Delta T$ are the same, it can be expected that the associated HF distributions show less dispersed values towards the high end and, thus, a shorter tail. In fact, Table 2 shows that percentile ratios associated with HF_{tot} definitions (bolded highlighted) are smaller than those associated with HF_n.

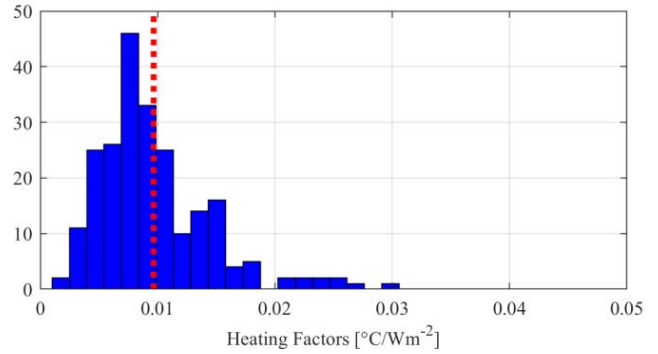


FIGURE 9. Occurrences distribution of HF_n avg.1. Red dotted line is the average value.

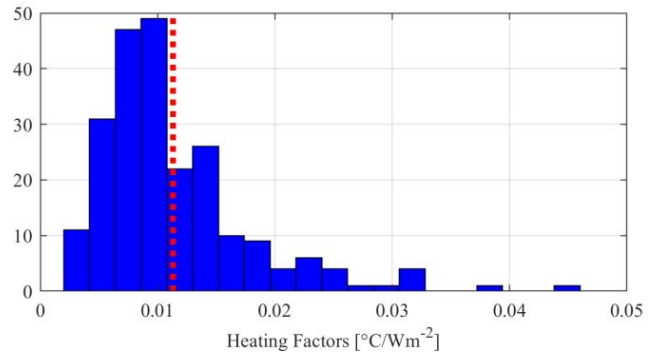


FIGURE 10. Occurrences distribution of HF_{tot} avg.1. Red dotted line is the average value.

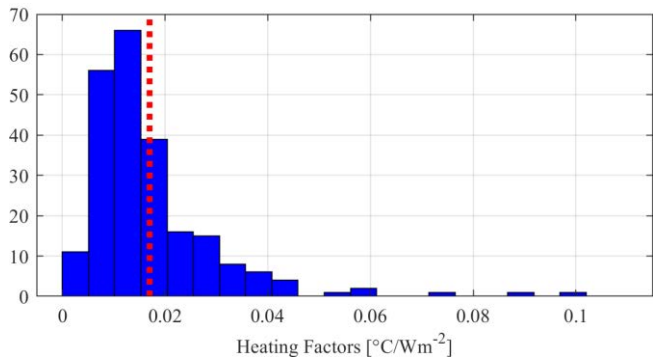


FIGURE 11. Occurrences distribution of HF_n avg.4. Red dotted line is the average value.

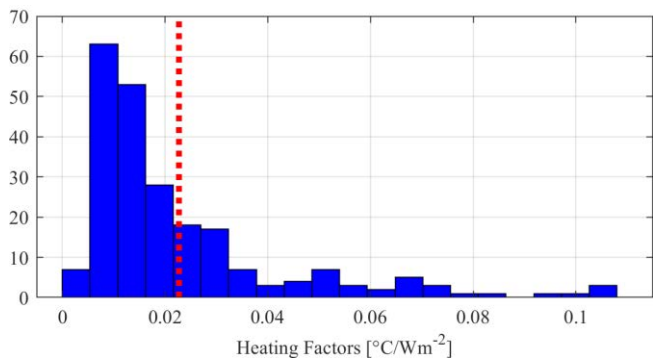


FIGURE 12. Occurrences distribution of HF_{tot} avg.4. Red dotted line is the average value.

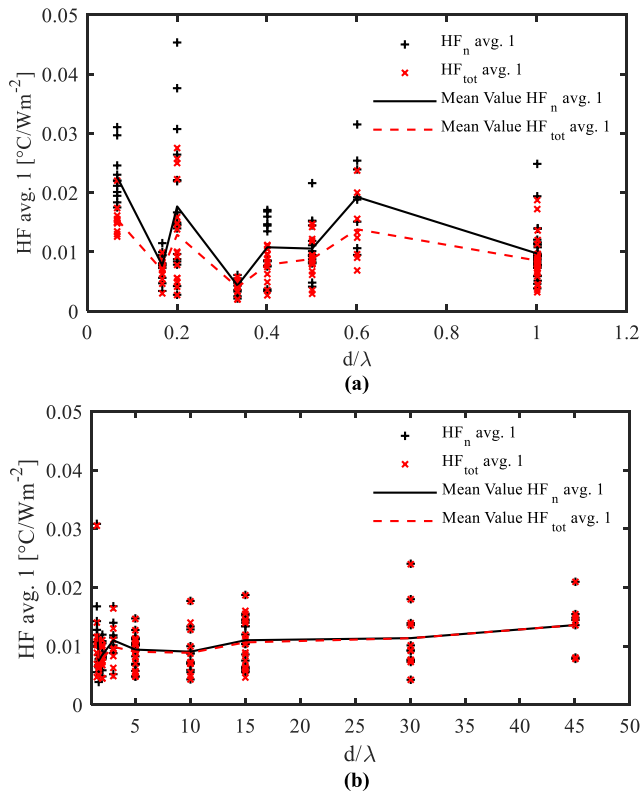


FIGURE 13. HF_n avg.1 (black) and HF_{tot} avg.1 (red) plotted vs. electric distance from 0 to 1 (a) and 1 to 45 (b). Continuous and dashed lines (same colours) link the average values of HF_n avg.1 and HF_{tot} avg.1.

Finally, the plots of the HF rearranged as a function of electric distance, i.e. the distance d over the wavelength λ , distinguished by the PD definitions (HF_n vs. HF_{tot}), are reported in Figs. 13 and 14 for the 1 cm² and 4 cm² averaging areas, respectively. The graphical evaluation of the plots shows that the average value of HF_n is consistently greater than the one of HF_{tot} , but this difference diminishes with electrical distance because the tangential components of the Poynting vector tend to vanish in the far-field. Instead, a greater dispersion is observed at distances $d \leq 0.6\lambda$ (see Figs. 13(a) and 14(a)) due to the near-field zone characteristics.

C. PEARSON CORRELATION COEFFICIENTS

Tables 3 and 4 show the computed values of Pearson correlation coefficients for the dipole source and directional antennas, respectively. In the first case, the PD metric with highest r_{jk} is the one related to the definition of sPD_{tot1} , while in the second case, coefficients related to sPD_{n1} are always higher, with the exception of the 10, 30 GHz data group, where the highest coefficients are r_{tot1} and r_{tot4} , respectively. This may be due to the increased capability to focus the beam for the directional antennas.

In addition, when grouping data by separation distance, all the highest r_{jk} values are obtained for $d \geq 5$ mm, except for r_{tot4} in the case of directional antennas at the highest

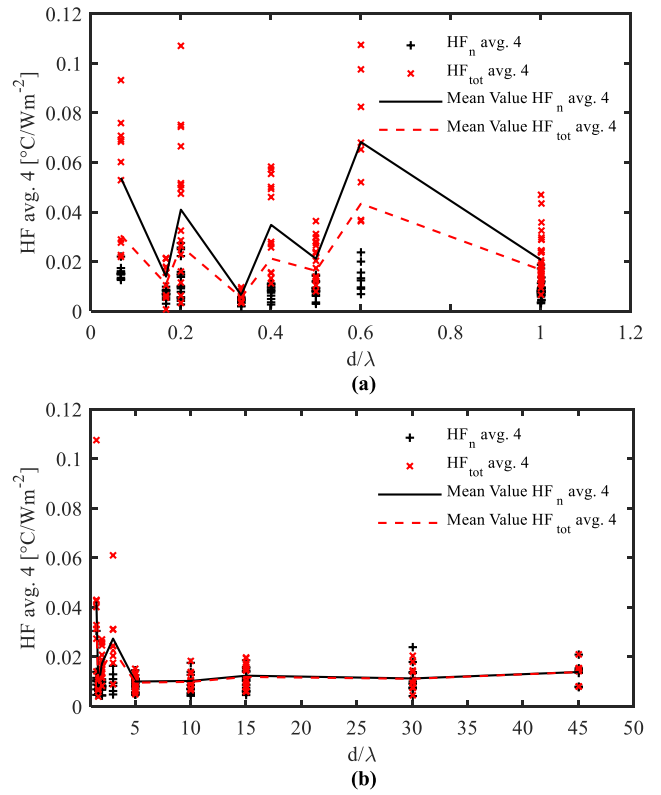


FIGURE 14. HF_n avg.4 (black) and HF_{tot} avg.4 (red) plotted vs. electric distance from 0 to 1 (a) and 1 to 45 (b). Continuous and dashed lines (same colours) link the average values of HF_n avg.4 and HF_{tot} avg.4.

frequencies, where including all distances in the analyses seems to yield higher correlation. In general, the increased correlation, obtained excluding the smallest distance, may be due to the reduced level of tangential components of the Poynting vector in the near-field compared to the reactive components. Finally, when grouping data by the frequency range, it can be observed, as expected, that both PD definitions with 1 cm² averaging area correlate better than the respective definitions with 4 cm² for the 60, 90 GHz data set, while this is not always true for the 10, 30 GHz data set.

D. STATISTICAL SIGNIFICANCE TEST

Tables 6 and 7 show the results of the z - and t -scores analyses considering the data related to 1 cm² and 4 cm² averaging areas, respectively. The input values provided to the *cocor* package in order to perform the significance test are reported in Table 5. In particular, it shows the correlation coefficients compared in pairs, i.e., r_{n1} , r_{tot1} and r_{n4} , r_{tot4} , and the associated coefficients $r_{n1,tot1}$ and $r_{n4,tot4}$, obtained computing the correlation of sPD_n avg.1 with sPD_{tot} avg.1 and sPD_n avg.4 with sPD_{tot} avg.4. A one-tailed test for the hypothesis that $r_n < r_{tot}$ has been performed.

The z - and t -scores reported in Tables 6 and 7 show that the results have strong statistical significance, with scores well below the critical values related to 95% confidence level. This result confirms that the correlation of the total component

TABLE 3. psPD vs. pΔT correlation coefficients related to the dipole source. Highlighted in bold are the highest values for each data set.

Dipole	<i>d</i>	<i>r_{n1}</i>	<i>r_{tot1}</i>	<i>r_{n4}</i>	<i>r_{tot4}</i>
All <i>f</i>	all	0.862	0.895	0.776	0.868
	≥ 5 mm	0.910	0.913	0.853	0.878
10, 30 GHz	all	0.831	0.874	0.754	0.856
	≥ 5 mm	0.921	0.922	0.858	0.883
60, 90 GHz	all	0.897	0.920	0.812	0.892
	≥ 5 mm	0.946	0.948	0.916	0.937

TABLE 4. psPD vs. pΔT correlation coefficients relate to the directional antennas. Highlighted in bold are the highest values for each data set.

Direct. Anten.	<i>d</i>	<i>r_{n1}</i>	<i>r_{tot1}</i>	<i>r_{n4}</i>	<i>r_{tot4}</i>
All <i>f</i>	all	0.806	0.805	0.637	0.769
	≥ 5 mm	0.870	0.837	0.705	0.700
10, 30 GHz	all	0.836	0.872	0.749	0.830
	≥ 5 mm	0.894	0.923	0.906	0.927
60, 90 GHz	all	0.833	0.709	0.579	0.643
	≥ 5 mm	0.858	0.796	0.580	0.576

TABLE 5. Input values for the *cocor* analysis. Highlighted in bold are the highest values for each data set.

Source	avg.	<i>r_n</i>	<i>r_{tot}</i>	<i>r_{n,tot}</i>
Dipole	1 cm ²	0.862	0.895	0.9869
	4 cm ²	0.776	0.868	0.9696
Directional	1 cm ²	0.806	0.805	0.9331
	4 cm ²	0.637	0.769	0.8121

with the peak temperature rise is (statistically) significantly higher than that of the normal component. In fact, all the employed tests led to the rejection of the null-hypothesis $r_n = r_{tot}$. The only exception to this trend comes from the comparison between r_{n1} and r_{tot1} for the directional antennas data, where the two correlations could not be distinguished at the 95% confidence level (see Table 5).

V. DISCUSSIONS

A. EXPLANATION OF THE OBTAINED RESULTS

The results of Table 3 show that, for the simple dipole source, the definition with sPD_{tot} presents highest values of correlation coefficients with temperature rise compared to the

TABLE 6. z-scores and t-scores of the psPD avg.1 and pΔT correlation comparison between data belonging to the dipole source and to the directional antennas. In the Null-Hypothesis column, *rej.* stands for rejected and *ret.* stands for retained.

sPD _n avg.1 vs. sPD _{tot} avg.1	z- or t- test	z- or t- score		Null-Hypothesis	
		Dipole	Direct.	Dipole	Direct.
Pearson and Filon's	z	-3.866	0.0156	<i>rej.</i>	<i>ret.</i>
Hotelling's	t	-5.046	0.0155	<i>rej.</i>	<i>ret.</i>
Williams'	t	-5.045	0.0154	<i>rej.</i>	<i>ret.</i>
Olkin's	z	-3.866	0.0156	<i>rej.</i>	<i>ret.</i>
Dunn and Clark's	z	-4.912	0.0154	<i>rej.</i>	<i>ret.</i>
Hendrickson et al.	t	-5.046	0.0155	<i>rej.</i>	<i>ret.</i>
Steiger's	z	-4.581	0.0154	<i>rej.</i>	<i>ret.</i>
Meng et al.	z	-4.578	0.0154	<i>rej.</i>	<i>ret.</i>
Hittner et al.	z	-4.563	0.0154	<i>rej.</i>	<i>ret.</i>

TABLE 7. z-scores and t-scores of the psPD avg.4 and pΔT correlation comparison between data belonging to the dipole source and to the directional antennas. In the Null-Hypothesis column, *rej.* stands for rejected and *ret.* stands for retained.

sPD _n avg.4 vs. sPD _{tot} avg.4	z- or t- test	z- or t- score		Null-Hypothesis	
		Dipole	Direct.	Dipole	Direct.
Pearson and Filon's	z	-5.188	-3.279	<i>rej.</i>	<i>rej.</i>
Hotelling's	t	-9.326	-3.638	<i>rej.</i>	<i>rej.</i>
Williams'	t	-9.322	-3.617	<i>rej.</i>	<i>rej.</i>
Olkin's	z	-5.188	-3.279	<i>rej.</i>	<i>rej.</i>
Dunn and Clark's	z	-8.332	-3.529	<i>rej.</i>	<i>rej.</i>
Hendrickson et al.	t	-9.326	-3.638	<i>rej.</i>	<i>rej.</i>
Steiger's	z	-7.141	-3.480	<i>rej.</i>	<i>rej.</i>
Meng et al.	z	-7.119	-3.468	<i>rej.</i>	<i>rej.</i>
Hittner et al.	z	-7.047	-3.456	<i>rej.</i>	<i>rej.</i>

definition sPD_n , both when grouping the data by separation distance and frequency. The small difference between the values of correlation coefficients corresponding to the two definitions indicates that both resulting quantities correlate strongly with temperature rise (correlation coefficients >0.7).

One possible explanation for this is that the scenarios considered in this study are mainly for the normal incidence of the field on the body, thus the differences are relatively small. However, this slightly better correlation with the total components may be attributed to the near-field exposure conditions, where some of the components are obliquely

incident to the model. Furthermore, excluding the data for the shortest distance of 2 mm, which is considered as near-field exposure (at least below 30 GHz), the correlation is generally improved. In other words, the correlation at 2 mm is very poor highlighting the limitation of IPD as RL/ERL metric at close distances.

Differently from the dipole, exposure to more complex sources yields to a less clear picture. In fact, while the power density and heating values corresponding to the dipole sources are consistent and do not show any particular clustering of values or alarming variability, the data coming from the simulations of directional antennas are obviously characterized by larger variations in the correlation coefficients (see Table 4) and by the presence of some outliers in their distribution. The latter can be found also in the scatter plots (see Figs. 5-8) with some $p\Delta T$ values between 2 and 2.5 °C. Considerations about possible health risks from such high temperature increases and conservative safety margins lie outside the scope of this work.

B. METHOD AND DATA COLLECTION LIMITATIONS

When conducting a statistical analysis, a crucial aspect is the analysis of the available set of data, both in terms of sample size and nature of the collected data. In particular, for the former aspect, it is a good practice to establish whether the size of the analyzed samples is sufficient to guarantee a certain significance of the statistics. In this study, it has been verified that all the chosen samples for both *dipole data* (115) and *directional antennas data* (112) were large enough to properly represent their respective statistical population of values. Specifically, an analysis on the tolerance limits conducted through *t*-statistics has shown that, at the 95% confidence level, the errors obtained by estimating the population means through the samples average falls between ~11.8% and ~16.4%.

Regarding the nature of the collected data, a critical aspect may be represented by the fact that they come from different organizations. However, a study of body model and thermal parameter variability impact for frequencies below 30 GHz was performed in [27] showing that the difference in *HF*s were globally below 20%. The authors of [27] concluded that, although the slight dependency on the body model, thermal parameters, and antenna models, the deviation of *HF*s is insignificant when considering the numerical methods used by different organizations.

VI. CONCLUSION

The observation of correlation coefficients, computed for the different data samples, shows that, in general, the spatial averaged power density metrics based on *total* components (i.e., magnitude) provide a slightly higher correlation than those based on the *normal* components. However, the difference is marginal (0.9 vs. 0.8) and the close values of correlation coefficients show that both definitions correlate with temperature elevation.

Moreover, the analysis of the heating factor distributions for different normal exposure configurations shows smaller relative standard deviation values when applying an sPD_{tot} definition. Consequently, this definition is expected to yield a slightly better estimate of the induced temperature increase than sPD_n . The observed difference is however not large and can mainly be attributed to near-field conditions.

Finally, the analysis of the statistical significance test confirmed that the PD definition using all *total* components correlates with temperature rise slightly better than the PD definition using the *normal* components (see Table 5). On the basis of the obtained results, we conclude that the sPD_{tot} is the definition that should be recommended as IPD metric in International exposure guidelines/standards for human protection.

ACKNOWLEDGMENT

The authors would like to thank Prof. Akimasa Hirata (Nagoya Institute of Technology) and Dr. Jafar Keshvari (Aalto University) and all IEEE/ICES/TC95/SC6 WG5 members for their valuable comments on this work.

REFERENCES

- [1] J. G. Andrews, S. Buzzi, W. Choi, S. V. Hanly, A. L. Lozano, A. C. Soong, and J. C. Zhang, "What will 5G be?" *IEEE J. Sel. Areas Commun.*, vol. 32, no. 6, pp. 1065–1082, Jun. 2014.
- [2] K. R. Foster, J. A. D'Andrea, S. Chalfin, and D. J. Hatcher, "Thermal modeling of millimeter wave damage to the primate cornea at 35 GHz and 94 GHz," *Health Phys.*, vol. 84, no. 6, pp. 764–769, Jun. 2003.
- [3] S. I. Alekseev, A. A. Radzievsky, M. K. Logani, and M. C. Ziskin, "Millimeter wave dosimetry of human skin," *Bioelectromagnetics*, vol. 29, no. 1, pp. 65–70, Jan. 2008.
- [4] M. Zhadobov, N. Chahat, R. Sauleau, C. Le Quement, and Y. L. Drean, "Millimeter-wave interactions with the human body: State of knowledge and recent advances," *Int. J. Microw. Wireless Technol.*, vol. 3, no. 2, pp. 237–247, 2011.
- [5] M. C. Ziskin, S. I. Alekseev, K. R. Foster, and Q. Balzano, "Tissue models for RF exposure evaluation at frequencies above 6 GHz," *Bioelectromagnetics*, vol. 39, no. 3, pp. 173–189, Apr. 2018.
- [6] International Commission on Non-Ionizing Radiation Protection (ICNIRP), "Guidelines for limiting exposure to time-varying electric, magnetic, and electromagnetic fields (100 kHz to 300 GHz)," *Health Phys.*, vol. 118, no. 5, pp. 483–524, 2020.
- [7] *IEEE Standard for Safety Levels With Respect to Human Exposure to Electric, Magnetic, and Electromagnetic Fields, 0 Hz to 300 GHz*, Standard IEEE-C95.1, 2019.
- [8] *Assessment of Power Density of Human Exposure to Radio Frequency Fields From Wireless Devices in Close Proximity to the Head and Body (Frequency Range of 6 GHz to 300 GHz)—Part I: Measurement Procedure, ED1*, Standard IEC/IEEE FDIS 63195-1, 2021.
- [9] *Assessment of Power Density of Human Exposure to Radio Frequency Fields From Wireless Devices in Close Proximity to the Head and Body (Frequency Range of 6 GHz to 300 GHz)—Part II: Computational Procedure, ED1*, Standard IEC/IEEE FDIS 63195-2, 2022.
- [10] A. Christ, T. Samaras, E. Neufeld, and N. Kuster, "Limitations of incident power density as a proxy for induced electromagnetic fields," *Bioelectromagnetics*, vol. 41, no. 5, pp. 348–359, May 2020.
- [11] S. Omi, K. Sasaki, and K. Wake, "Performance analysis of incident power density evaluation by inverse source method for compliance assessment at quasi-millimeter and millimeter wave bands," *IEEE Trans. Electromagn. Compat.*, vol. 63, no. 5, pp. 1649–1657, Oct. 2021.
- [12] Y. Diao, E. A. Rashed, and A. Hirata, "Assessment of absorbed power density and temperature rise for nonplanar body model under electromagnetic exposure above 6 GHz," *Phys. Med. Biol.*, vol. 65, no. 22, Nov. 2020, Art. no. 224001.

- [13] D. Funahashi, A. Hirata, S. Kodera, and K. R. Foster, "Area-averaged transmitted power density at skin surface as metric to estimate surface temperature elevation," *IEEE Access*, vol. 6, pp. 77665–77674, 2018.
- [14] K. R. Foster, M. C. Ziskin, and Q. Balzano, "Thermal modeling for the next generation of radiofrequency exposure limits: Commentary," *Health Phys.*, vol. 113, no. 1, pp. 41–53, 2017.
- [15] A. Hirata, D. Funahashi, and S. Kodera, "Setting exposure guidelines and product safety standards for radio-frequency exposure at frequencies above 6 GHz: Brief review," *Ann. Telecommun.*, vol. 74, nos. 1–2, pp. 17–24, Feb. 2019.
- [16] Y. Hashimoto, A. Hirata, R. Morimoto, S. Aonuma, I. Laakso, K. Jokela, and K. R. Foster, "On the averaging area for incident power density for human exposure limits at frequencies over 6 GHz," *Phys. Med. Biol.*, vol. 62, no. 8, pp. 3124–3138, Apr. 2017.
- [17] K. Foster and D. Colombi, "Thermal response of tissue to RF exposure from canonical dipoles at frequencies for future mobile communication systems," *Electron. Lett.*, vol. 53, no. 5, pp. 360–362, Mar. 2017.
- [18] W. He, B. Xu, Y. Yao, D. Colombi, Z. Ying, and S. He, "Implications of incident power density limits on power and EIRP levels of 5G millimeter-wave user equipment," *IEEE Access*, vol. 8, pp. 148214–148225, 2020.
- [19] T. Nakae, D. Funahashi, J. Higashiyama, T. Onishi, and A. Hirata, "Skin temperature elevation for incident power densities from dipole arrays at 28 GHz," *IEEE Access*, vol. 8, pp. 26863–26871, 2020.
- [20] K. Sasaki, K. Li, J. Chakrothai, T. Iyama, T. Onishi, and S. Watanabe, "Error analysis of a near-field reconstruction technique based on plane wave spectrum expansion for power density assessment above 6 GHz," *IEEE Access*, vol. 7, pp. 11591–11598, 2019.
- [21] W. He, B. Xu, M. Gustafsson, Z. Ying, and S. He, "RF compliance study of temperature elevation in human head model around 28 GHz for 5G user equipment application: Simulation analysis," *IEEE Access*, vol. 6, pp. 830–838, 2018.
- [22] D. Colombi, B. Thors, C. Törnevik, and Q. Balzano, "RF energy absorption by biological tissues in close proximity to mmW 5G wireless equipment," *IEEE Access*, vol. 6, pp. 4974–4981, 2018.
- [23] B. Thors, D. Colombi, Z. Ying, T. Bolin, and C. Törnevik, "Exposure to RF EMF from array antennas in 5G mobile communication equipment," *IEEE Access*, vol. 4, pp. 7469–7478, 2016.
- [24] Y. Diao, K. Li, K. Sasaki, S. Kodera, I. Laakso, W. E. Hajj, and A. Hirata, "Effect of incidence angle on the spatial-average of incident power density definition to correlate skin temperature rise for millimeter wave exposures," *IEEE Trans. Electromagn. Compat.*, vol. 63, no. 5, pp. 1709–1716, Oct. 2021.
- [25] K. Li, K. Sasaki, S. Watanabe, and H. Shirai, "Relationship between power density and surface temperature elevation for human skin exposure to electromagnetic waves with oblique incidence angle from 6 GHz to 1 THz," *Phys. Med. Biol.*, vol. 64, no. 6, Mar. 2019, Art. no. 065016.
- [26] T. Samaras and N. Kuster, "Theoretical evaluation of the power transmitted to the body as a function of angle of incidence and polarization at frequencies > 6 GHz and its relevance for standardization," *Bioelectromagnetics*, vol. 40, no. 2, pp. 136–139, Jan. 2019.
- [27] K. Li, Y. Diao, K. Sasaki, A. Prokop, D. Poljak, V. Doric, J. Xi, S. Kodera, A. Hirata, and W. E. Hajj, "Intercomparison of calculated incident power density and temperature rise for exposure from different antennas at 10–90 GHz," *IEEE Access*, vol. 9, pp. 151654–151666, 2021.
- [28] K. R. Foster, M. C. Ziskin, Q. Balzano, and G. Bit-Babik, "Modeling tissue heating from exposure to radiofrequency energy and relevance of tissue heating to exposure limits: Heating factor," *Health Phys.*, vol. 115, no. 2, pp. 295–307, 2018.
- [29] R. E. Walpole, R. H. Myers, S. L. Myers, and K. Ye, *Probability and Statistics for Engineers and Scientists*, vol. 5. New York, NY, USA: Macmillan, 1993.
- [30] B. Diedenhofen and J. Musch, "Cocor: A comprehensive solution for the statistical comparison of correlations," *PLoS ONE*, vol. 10, no. 4, Apr. 2015, Art. no. e0121945.



VALERIO DE SANTIS (Senior Member, IEEE) received the Laurea degree (Hons.) in telecommunication engineering and the Ph.D. degree in electrical and computer engineering from the University of L'Aquila, L'Aquila, Italy, in 2006 and 2010, respectively.

He joined the Foundation for Research on Information Technologies in Society, IT²IS Foundation, Switzerland, from 2011 to 2013, holding the position of the Project Leader. He was an Assistant Professor at the Nagoya Institute of Technology, Nagoya, Japan, from January to March 2015. He is currently an Associate Professor at the University of L'Aquila. His current research interests include wireless power transfer, numerical methods and techniques, electromagnetic compatibility, and human exposure safety.

Prof. De Santis is participating and leading several standardization efforts in the human exposure and product safety domain. He is a member of IEC TC 106 and IEEE ICES TC95. He received the Second Best Student Paper Award at the Bioelectromagnetics Society (BEMS) Annual Meeting, Cancun, Mexico, in 2006, the Best Student Paper Award at the IEEE International Symposium on EMC, Honolulu, USA, in 2007, and the Leo L. Beranek Travel Grant at the IEEE International Symposium on EMC, Detroit, USA, in 2008.



ANTONIO DI FRANCESCO received the Laurea degree (Hons.) in mechanical engineering and the Laurea Magistrale degree (Hons.) in mathematical engineering from the University of L'Aquila, L'Aquila, Italy, in 2017 and 2020, respectively, where he is currently pursuing the Ph.D. degree in mathematics and models.

His current research interests include the physical and mathematical modeling and computer simulation of bioheat conduction and thermal effects of EM fields on biological tissues, nonequilibrium statistical physics, and in stochastic modeling of physical and biological phenomena.



GIORGI BIT-BABIK (Senior Member, IEEE) received the M.Sc. (Hons.) and Ph.D. degrees in radio physics and electronics from Tbilisi State University (TSU), Tbilisi, Georgia, in 1994 and 1998, respectively.

He was a Research Staff Member and later an Associate Professor at TSU. In 2001, he joined the Electromagnetic Energy (EME) Research Laboratory, Motorola Inc., Fort Lauderdale, FL, USA. He is currently a Distinguished Member of Technical Staff and the Science Advisory Board Associate at Motorola Solutions Inc. His work is related to antenna technology research and development, RF exposure dosimetry, and compliance assessment and standards. He holds 30 patents mostly in antenna technology and has over 90 journals and conference publications in applied electromagnetics and RF exposure dosimetry.

Dr. Bit-Babik is actively involved in the IEEE ICES TC34 and IEC TC106 standards committees developing measurement and numerical methods for RF exposure assessment. He is a member of multiple working groups and project teams within ICES TC34 and TC106, a Convenor of the JWG IEC/IEEE 62704-2, and also serves as a Technical Advisor of the USNC TAG106. He was a recipient of the IEC 1906 Award and IEEE Standards Association International Award.



JOHN ROMAN (Senior Member, IEEE) was born in Dallas, TX, USA, in 1961. He received the B.S. degree in electrical engineering and the M.S. degree in electrical engineering with a focus on antenna theory from Florida Atlantic University (FAU), Boca Raton, FL, USA, in 1988 and 1998, respectively.

He was a Research Faculty Member at FAU, from 1990 to 1995, as the Associate Director of the EMI Research and Development Laboratory, the Compliance Manager of ECI Telecom, from 1995 to 2000, and joined Intel Corporation, in 2000, where he is currently the Director of Broadband and Regulatory Policy at Intel Corporation, Hillsboro, OR, USA.

Mr. Roman is also a member of the 5G Automotive Association, where he is the Vice Chair of the Regulatory Working Group. He is currently the Co-Convenor of IEC/IEEE 63195-2 ED1, Assessment of Power Density of Human Exposure to Radio Frequency Fields from Wireless Devices in Close Proximity to the Head and Body (Frequency Range Of 6 GHz To 300 GHz)—Part 2: Computational Procedure. He has published several papers in IEEE journals and conference proceedings, for example most recently such as Teruo Onishi; Kai Niskala; Andreas Christ; John Roman, Exposure assessment methods with respect to the 5G mobile communication systems, and 2020 International Symposium on Electromagnetic Compatibility—EMC EUROPE, in September 2020.



WALID EL HAJJ (Member, IEEE) received the master's degree (Research) in microwave materials and devices for communication systems and the Ph.D. degree in information and communications sciences and technologies from Telecom Bretagne, Brest, France, in 2008 and 2011, respectively.

From 2011 to 2013, he was a Researcher with the LabSTICC/MOM Laboratory, Microwave Department, Telecom Bretagne. He joined Intel Corporation, in 2014. He is currently a Scientist Officer at the Intel Wireless RF Laboratory (ISO 17025 Certification Laboratory), Wireless Test and Certification Center Group. He is leading the different research and development activities related to new wireless technologies and products certification.

Dr. El Hajj is participating and leading several standardization efforts in the human exposure and product safety domain. He is mandated as an Expert in French Standardization Association (AFNOR). Since 2017, he has been participating in the development of several IEEE/IEC standards on human exposure computational and measurement assessments. He is a member of IEC TC 106 and IEEE ICES TC95. He is the Convener of Working Group five under Subcommittee six of IEEE ICES TC95 established to study the different aspects of incident power density definition in correlation with temperature elevation. He is also a member of CMC TF Radio Group in IECEE.

• • •